ISSN: 0975-833X

Available online at http://www.journalcra.com

International Journal of Current Research
Vol. 14, Issue, 06, pp.21788-21795, June, 2022
DOI: https://doi.org/10.24941/ijcr.43681.06.2022

INTERNATIONAL JOURNAL OF CURRENT RESEARCH

REVIEW ARTICLE

MILLIMETER WAVE ATTENUATION BY FLAT SEA-SURFACE COVERED BY FOAM USING FINITE DIFFERENCE ALGORITHM OF PARABOLIC EQUATION METHOD

***Aguiyi Nduka Watson, Godday Biowei and Ayibapreye Kelvin Benjamin**

Department of Electrical, Electronic Engineering, Niger Delta University

ARTICLE INFO

Article History:
Received 14th March, 2022
Received in revised form
19th April, 2022
Accepted 25th May, 2022
Published online 30th June, 2022

Key words:

Millimeter wave, attenuation, flat sea-surface, foam, finite difference method.

Corresponding Author:
Ayibapreye Kelvin Benjamin

ABSTRACT

In this letter, millimeter wave attenuation by flat sea surface covered by foam is reported. This was achieved by developing an analytical model of foam-covered sea surface using the finite difference method (FDM) method, which is a solution to the Parabolic Wave Equation (PWE) method. The PWE has been widely used to solving Electromagnetic (EM) wave extinction and radio wave propagation in random media problems. The FDM method investigates attenuation of EM waves propagating through slices of sea foam layer as functions of frequency, foam layer thickness, polarization and angle of incidence. Results obtainedshowed that attenuation increases with the depth of sea foam layers and decreases with increase in propagation angle for various WindSat frequencies.

Citation: ***Aguiyi Nduka Watson, Godday Biowei and Ayibapreye Kelvin Benjamin.*** **2022.** "Millimeter Wave Attenuation by Flat Sea-surface covered by Foam using Finite Difference Algorithm of Parabolic Equation Method*". International Journal of Current Research*, 14, (06), 21788-21795.

INTRODUCTION

The parabolic wave equation is a one-way outgoing wave propagation model which is derived from the Helmholtz wave equation. The Helmholtz equation is obtained by decoupling of Maxwell's equations (1,2). Tappert was first to suggest the split-step Fourier solution for solving PE models. The split-step Fourier method was historically proposed initially by Tappert (3) in the early 1970s to solve the non-linear Korteweg-de Vries (Kdv) wave equation with constant coefficients. Hardin and Tappert presented a further application of the split-step Fourier transform (SSFT) solution to non-linear and variable coefficient wave equations (4). Tappert (2) illustrated that the SSFT method is accurate and unconditionally stable for solving parabolic wave equation with variable coefficient. The split-step algorithm has been extensively used to solve the SPE ever since it was developed by Hardin and Tappert (2) in the early 1970s. The technique is computationally efficient for long-range, narrow-angle propagation problems with negligible bottom interactions. Reflection and refraction effects of millimeter wave (mmW) due to its interaction with densely packed particles (air-bubbles) are physical oceanographic and marine geological features. In many scenarios, the three dimensional ($3D$) models are adequate for accurate predictionof electromagnetic wave (EM) field propagation through random media. Tolstoy (4) reported a variety of $3D$ modelling techniques for describing EM wave propagationthrough random media over the past decades. In this article, we adopt the parabolic equation (PE)method, which was introduced by Tappert in the early 1970s for two dimensional ($2D$) one-way EM wave propagation problems. The PE Method is very effective and efficient in modelling long-range EM wave propagation in the ocean.For short-range, deep-water problems and shallow water problems in general, propagation is basically more wide-angled and bottom interacting paths become more important. The principal advantages of the various parabolic wave equations derived below is that it constitutes an initial value problem in range and hence can be solved by a range marching numerical technique, given a source field distribution over depth at the initial range. Over the years, several different solution techniques have been implemented in computer codes (5), but only the split-step Fourier technique and various finite-difference/finite-element techniques have gained widespread use in the underwater acoustic community. Before going into details on the numerical solution schemes, let us briefly point out some advantages and disadvantages of these two main solution techniques.

This requires the use of wide-angle PEs, which can be solved only by finite difference or finite elements. Moreover, the strong speed and density contrasts encountered at the water-bottom interface adversely affect the computational efficiency of the split-step technique, which in cases of strong bottom interaction requires an excessively fine computational grid $(\Delta x, \Delta z)$. Hence, the advantage of higher computational efficiency of the split-step technique is entirely lost in situations with strong bottom interactions. Finite-difference and Finite-element solutions are applicable to PE for arbitrary large angles. The main drawback of these schemes is that, for long range the split-step solution is more efficient and also for narrow angle with minimal or no bottom interaction. The split-step solution remains the most adopted technique for performance prediction as it is more suitable to solving many practical ocean-surface problems. Conversely, the finite-difference and finite-element schemes have widespread application for wide-angle and bottom interacting boundaries. It is prominent for providing higher accuracy in these domains.
The most recent development in terms of efficient PE solution schemes is a split-step Pade' approximations derived by Collins (6). He uses higher order Pade' approximations not the square root operators. The result is a considerable efficiency gain through the use of higher range step. Thus, the scheme is claimed to be more than an order of magnitude faster than standard FD/FE solution techniques. This could create a unified PE solution approach where the accurate high angle PEs can be solved with the efficiency of the classical split-step Fourier scheme.

The FDM routine was implemented to propagate the plane wave

$$E(z_0, x, y) = E(z, x, y) exp\left(ik_x + ik_y + ik_z z\right)$$

with $E(z, x, y) \approx 1$ along the forward $+z$ direction. The plane wave was propagated through five (5) 2D slices of sea foam layers each containing isotropically distributed bubbles. The slices are equally dimensioned with area $100\ mm \times 50\ mm$ with depth of foam layers$\delta_t = 10\ mm$ separating adjacent layers. The foam layer thickness d $\gg \lambda_0$ is required to account for attenuation (E-field amplitude variation) and diffuse scattering (E-field phase variation) as the incident E-field travelsthrough slices of the sea foam layer.WindSat frequency channels $(6.8\ GHz, 10.7\ GHz, 18.7\ GHz, 23.8\ GHz, 37\ GHz)$ were used for propagation of the E-field through slices of sea foam layers. The incident wave is tilted from the normal so that there is an initial phase gradient along the surface of the sea foam model. This is done by assigning values of $0 \leq \theta_i \leq 60^\circ$for the zenith angle and fixed azimuthal angle of $\emptyset = 0^\circ$.

For each of the angles θ_i we compute the E-fieldthat emerges from the foam layers and calculate the attenuation α_{dB} through the foam layers and back to the sea surface. This was modelled using finite difference algorithm of the parabolic equation described below.

Finite Difference Algorithm of Parabolic Equation

The wide-angled and exponential pseudo-differential operator was approximated using a sum of Padé$(1,1)$ functions as

$$f(\sigma, x) = \exp\left(\sigma(\sqrt{1+x})\right) \tag{1}$$

This is a function of the variable x, with complex parameter σ. Implementing a Taylor series expansion of the function f in terms of the variable x, about the point $x = 0$ yields

$$f(\sigma, x) = \exp(\sigma)\left\{1 + \frac{\sigma}{2}x + \frac{\sigma(\sigma-1)}{4}\frac{x^2}{2!} + \frac{1}{8}(3\sigma - 3\sigma^2 + \sigma^3)\frac{x^3}{3!} + \frac{1}{16}(-15\sigma + 15\sigma^2 - 6\sigma^3 + \sigma^4)\frac{x^4}{4!} + 0(x^5)\right\} \tag{2}$$

$$f_1(\sigma, x) = \exp(\sigma)\frac{1+ax}{1+bx} \tag{3}$$

where $\sigma = ik_0\Delta z$

The Padé$(1,1)$ formula is obtained by matching the Taylor expressions to degree two (2) of f and f_1. This is nicely done as shown

$$\frac{1+ax}{1+bx} = 1 + \frac{\sigma}{2}x + \frac{\sigma(\sigma-1)}{4}\frac{x^2}{2!} + 0(x^3) \tag{4}$$

The Padé$(1,1)$ coefficients a and b are

$$a = \frac{1+\sigma}{4}, b = \frac{1-\sigma}{4} \tag{5}$$

The approximation $f_1(\sigma, x)$ can be expressed in terms of Padé coefficients a and b

$$f_1(\sigma, x) = \exp\,(\sigma(\sqrt{1+x})) = \exp\,(\sigma)\frac{1+\frac{1+\sigma}{4}x}{1+\frac{1-\sigma}{4}x} \tag{6}$$

The Split-step formal matching expression is as shown

$$u(z+\Delta z, x) = \frac{1+\frac{1+\sigma}{4}x}{1+\frac{1-\sigma}{4}x}u(z, x \tag{7}$$

The implicit numerical integration scheme of (7) is given as

$$\left\{1+\frac{1-\sigma}{4}x\right\}u^{n+1} = \left\{1+\frac{1+\sigma}{4}x\right\}u^{n} \tag{8}$$

This was achieved by central finite differencing of the depth operator Z_h with respect to the depth variable z. The depth variable is discretized as $z = z + (1/2)\Delta z$.

$$(1+bZ_h)u^{n+1} = (1+aZ_h)u^n \tag{9}$$

Further algebraic expression of (9) yields

$$u^{n+1} + bZ_h u^{n+1} = u^n + aZ_h u^n \tag{10}$$

Expression of $Z_h u^{n+1}$ and $Z_h u^n$ as sum of second-order partial differential equation and dielectric constant of the media is given below

$$Z_h u^{n+1} = \frac{1}{k^2}\frac{\partial^2 u^{n+1}}{\partial z^2} + (n^2-1)u^{n+1} \tag{11}$$

$$Z_h u^{n} = \frac{1}{k^2}\frac{\partial^2 u^{n}}{\partial z^2} + (n^2-1)u^{n} \tag{12}$$

Applying second-order finite central difference method yields

$$\frac{\partial^2 u(z_i, x_n)}{\partial z^2} = \frac{-u_{i+2}^{n+1}+16u_{i+1}^{n+1}-30u_i^{n+1}+16u_{i-1}^{n+1}-u_{i-2}^{n+1}}{12\Delta z^2} \tag{13}$$

Substituting the expression for $\frac{\partial^2 u(z_i, x_n)}{\partial z^2}$ in (13) into (11) yields

$$Z_h u^{n+1} = \frac{1}{12k^2\Delta z^2}\{-u_{i+2}^{n+1} + 16u_{i+1}^{n+1} - 30u_i^{n+1} + 16u_{i-1}^{n+1} - u_{i-2}^{n+1}\} + (n^2-1)u_i^{n+1} \tag{14}$$

Where $A = \frac{1}{12k^2\Delta z^2}$ and $C = (n^2-1)$, (14) becomes

$$Z_h u^{n+1} = A\{-u_{i+2}^{n+1} + 16u_{i+1}^{n+1} - 30u_i^{n+1} + 16u_{i-1}^{n+1} - u_{i-2}^{n+1}\} + Cu_i^{n+1} \tag{15}$$

and can be further expressed as

$$Z_h u^{n+1} = -Au_{i+2}^{n+1} + 16Au_{i+1}^{n+1} - 30Au_i^{n+1} + Cu_i^{n+1} + 16Au_{i-1}^{n+1} - Au_{i-2}^{n+1} \tag{16}$$

Substituting $Z_h u^{n+1}$ in (16) into the left-hand side (LHS) of (10) gives

$$u_i^{n+1} + b_1\{-Au_{i+2}^{n+1} + 16Au_{i+1}^{n+1} - 30Au_i^{n+1} + Cu_i^{n+1} + 16Au_{i-1}^{n+1} - Au_{i-2}^{n+1}\} \tag{17}$$

which is further expressed as

$$u_i^{n+1} + -b_1Au_{i+2}^{n+1} + 16b_1Au_{i+1}^{n+1} - 30Ab_1u_i^{n+1} + b_1Cu_i^{n+1} + 16b_1Au_{i-1}^{n+1} - b_1Au_{i-2}^{n+1} \tag{18}$$

Taking like terms we obtain

$$-b_1Au_{i+2}^{n+1} + 16b_1Au_{i+1}^{n+1}(-30b_1A + b_1C + 1)u_i^{n+1} + 16b_1Au_{i-1}^{n+1} - b_1Au_{i-2}^{n+1} \tag{19}$$

Similarly, $Z_h u_i^n$ can be expressed as

$$Z_h u_i^n = A\{-u_{i+2}^n + 16u_{i+1}^n - 30u_i^n + 16u_{i-1}^n - u_{i-2}^n\} + Cu_i^n \tag{20}$$

and

$$u_i^n + Z_h u_i^n = u_i^n + a_1\{-Au_{i+2}^n + 16Au_{i+1}^n - 30Au_i^n + Cu_i^n + 16Au_{i-1}^n - Au_{i-2}^n\} \tag{21}$$

substituting equation (21) into the right-hand side (RHS) of (20) yields

$$u_i^n - a_1Au_{i+2}^n + 16a_1Au_{i+1}^n - 30a_1Au_i^n + a_1Cu_i^n + 16a_1Au_{i-1}^n - a_1Au_{i-2}^n \tag{22}$$

Taking like terms gives

$$-a_1Au_{i+2}^n + 16a_1Au_{i+1}^n + (-30a_1A + a_1C + 1)u_i^n + 16a_1Au_{i-1}^n - a_1Au_{i-2}^n \tag{23}$$

Let's denote $\alpha = -a_1A, \beta = 16a_1A, \gamma = (-30a_1A + a_1C + 1), \zeta = -b_1A, \eta = 16b_1A$ and $\lambda = (-30b_1A + b_1C + 1)$

Therefore, equation (23) becomes

$$\alpha u_{i+2}^{n+1} + \beta u_{i+1}^{n+1} + \gamma u_i^{n+1} + \beta u_{i-1}^{n+1} + \alpha u_{i-2}^{n+1} = \zeta u_{i+2}^n + \eta u_{i+1}^n + \lambda u_i^n + \eta u_{i-1}^n + \zeta u_{i-2}^n \tag{24}$$

Equation (24) in matrix form is written as

$$U_{n+1} = Y_m U_n \tag{25}$$

where X_m and Y_m are $m \times m$ pentadiagonal or tridiagonal matrices while U_{n+1} and U_n are column vectors of same dimension m. The animated form of (25) is shown below.

$$\begin{pmatrix} \gamma & \beta & \alpha & 0 & 0 & 0 & 0 \\ \beta & \gamma & \beta & \alpha & 0 & 0 & 0 \\ \alpha & \beta & \gamma & \beta & \alpha & 0 & 0 \\ 0 & \alpha & \beta & \gamma & \beta & \alpha & 0 \\ 0 & 0 & \alpha & \beta & \gamma & \beta & \alpha \\ 0 & 0 & 0 & \alpha & \beta & \gamma & \beta \\ 0 & 0 & 0 & 0 & \alpha & \beta & \gamma \end{pmatrix} \begin{pmatrix} u_{i+1}^{n+1} \\ u_{i+1}^{n+1} \\ \cdot \\ \cdot \\ \cdot \\ \cdot \\ u_{i-N}^{n+1} \end{pmatrix} = \begin{pmatrix} \lambda & \eta & \zeta & 0 & 0 & 0 & 0 \\ \eta & \lambda & \eta & \zeta & 0 & 0 & 0 \\ \zeta & \eta & \lambda & \eta & \zeta & 0 & 0 \\ 0 & \zeta & \eta & \lambda & \eta & \zeta & 0 \\ 0 & 0 & \zeta & \eta & \lambda & \eta & \zeta \\ 0 & 0 & 0 & \zeta & \eta & \lambda & \eta \\ 0 & 0 & 0 & 0 & \zeta & \eta & \lambda \end{pmatrix} \begin{pmatrix} u_{i+1}^{n} \\ u_{i+1}^{n} \\ \cdot \\ \cdot \\ \cdot \\ \cdot \\ u_{i-N}^{n} \end{pmatrix} \qquad (26)$$

The solution to (26) is obtained by solving two pentadiagonal matrices. This can be solved using Gaussian elimination method, LU decomposition, inverse method, Jacobi's method, Gauss Siedel method, etc. Here, equation (26) was reduced by the matrix-vector product of Y_m and U_n to obtain $(Ax = b)$ expressed in block matrix form as given below.

$$(A)(x) = (b) \qquad (27)$$

The input parameters of algorithm comprise of $A(m \times m)$ non-singular square matrix and vector $b(m \times 1)$ on the RHS in the animation, the output solution vector is expressed as $x(m \times 1)$ returned at the end of the routine. The square pentadiagonal matrix A have entries $\gamma, \beta,$ and α while b have $\lambda, \eta,$ and ζ. The parameters $\gamma,\ \beta,$ and α were pre-computed using the expressions below.

$$\begin{pmatrix} a_{1,1}a_{1,2} & \cdots & a_{1,m} \\ a_{2,1}a_{2,2} & \cdots & a_{2,m} \\ \vdots & & \vdots \\ a_{2,1}a_{2,2} & \cdots & a_{2,m} \end{pmatrix} = \begin{pmatrix} 1 & & & \\ l_{2,1} & 1 & & \\ \vdots & \vdots & \ddots & \\ l_{m,1}l_{m,2} & \cdots & & 1 \end{pmatrix} \begin{pmatrix} u_{1,1}u_{1,2} & \cdots & u_{1,m} \\ & u_{2,2} & \cdots & u_{2,m} \\ & & \ddots & \vdots \\ & & & u_{m,m} \end{pmatrix} \qquad (28)$$

RESULTS AND DISCUSSION

Attenuation of field intensity $|E|^2$ as a function of depth of seafoam layer, frequency and propagation angle.

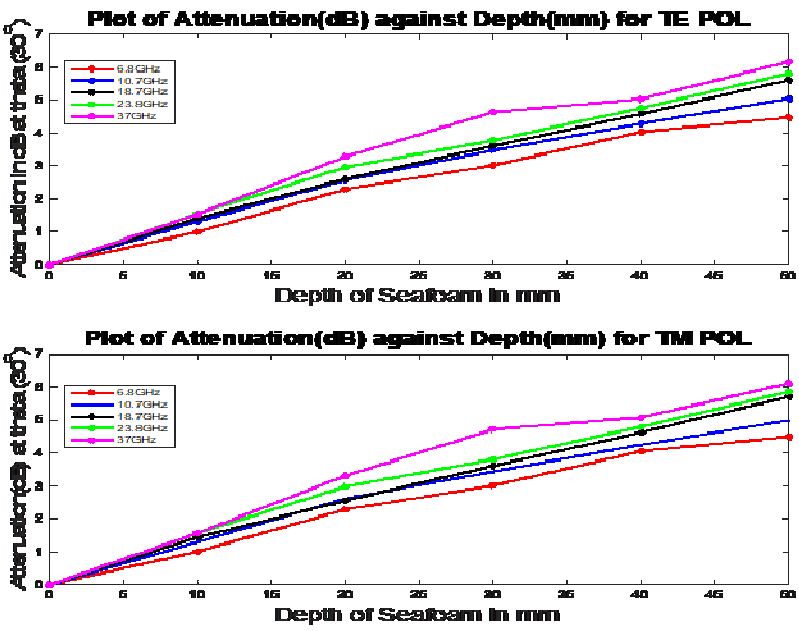

Figure 1. Attenuation (dB) of field intensity $|E|^2$ for TE and TM polarization against depth of sea foam with zenith $\theta_i = 30°$ and azimuth $\emptyset = 0°$for thin phase scattering screens.

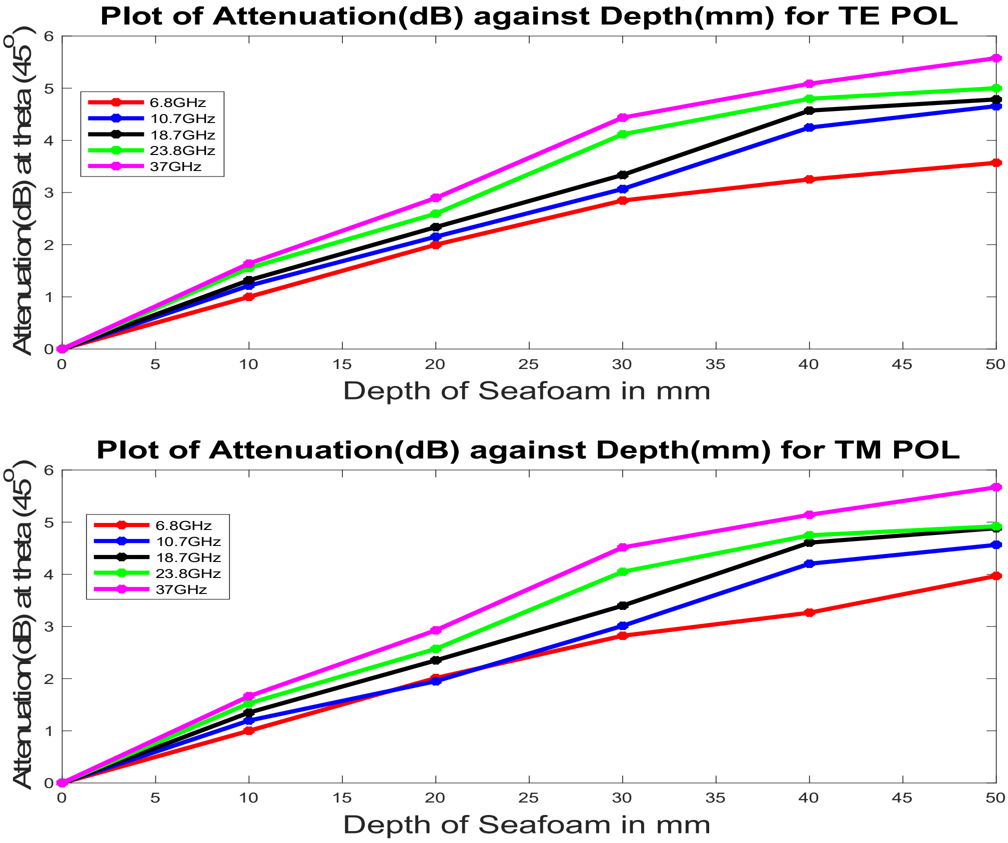

Figure 2. Attenuation (dB) of field intensity $|E|^2$ for TE and TM polarization against depth of sea foam with zenith $\theta_i = 45°$ and azimuth $\emptyset = 0°$ for thin phase scattering screen

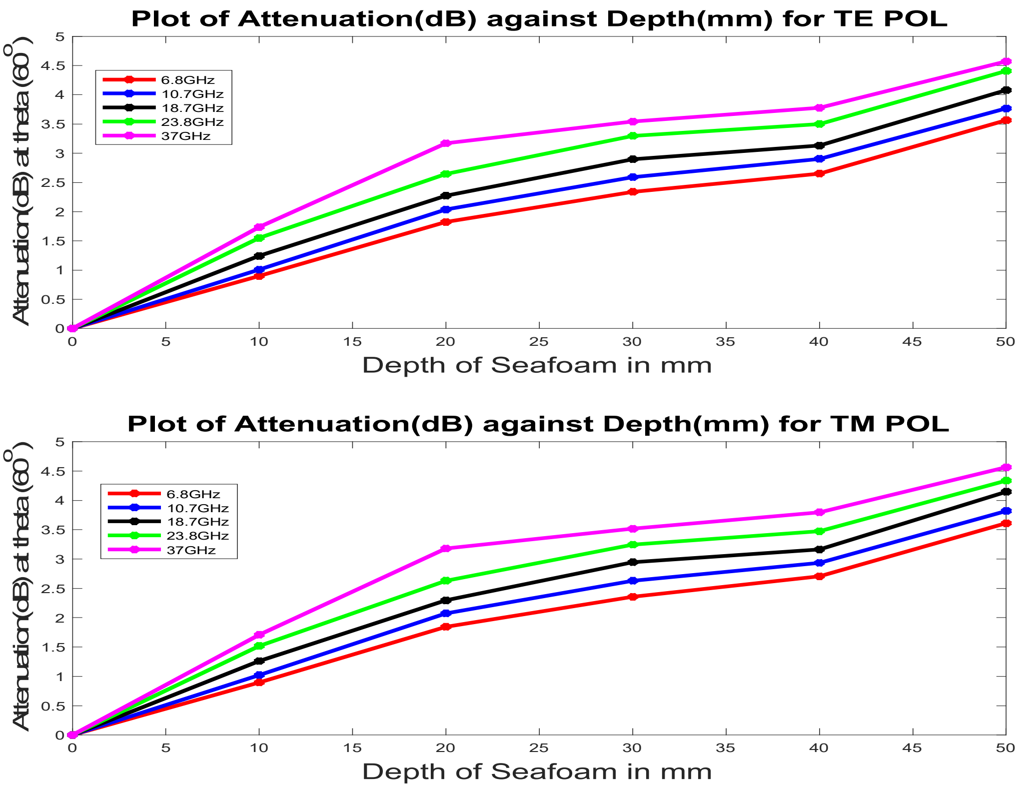

Figure 3. Attenuation (dB) of field intensity $|E|^2$ for TE and TM polarization against depth of sea foam with zenith $\theta_i = 60°$ and azimuth $\emptyset = 0°$ for thin phase scattering screens.

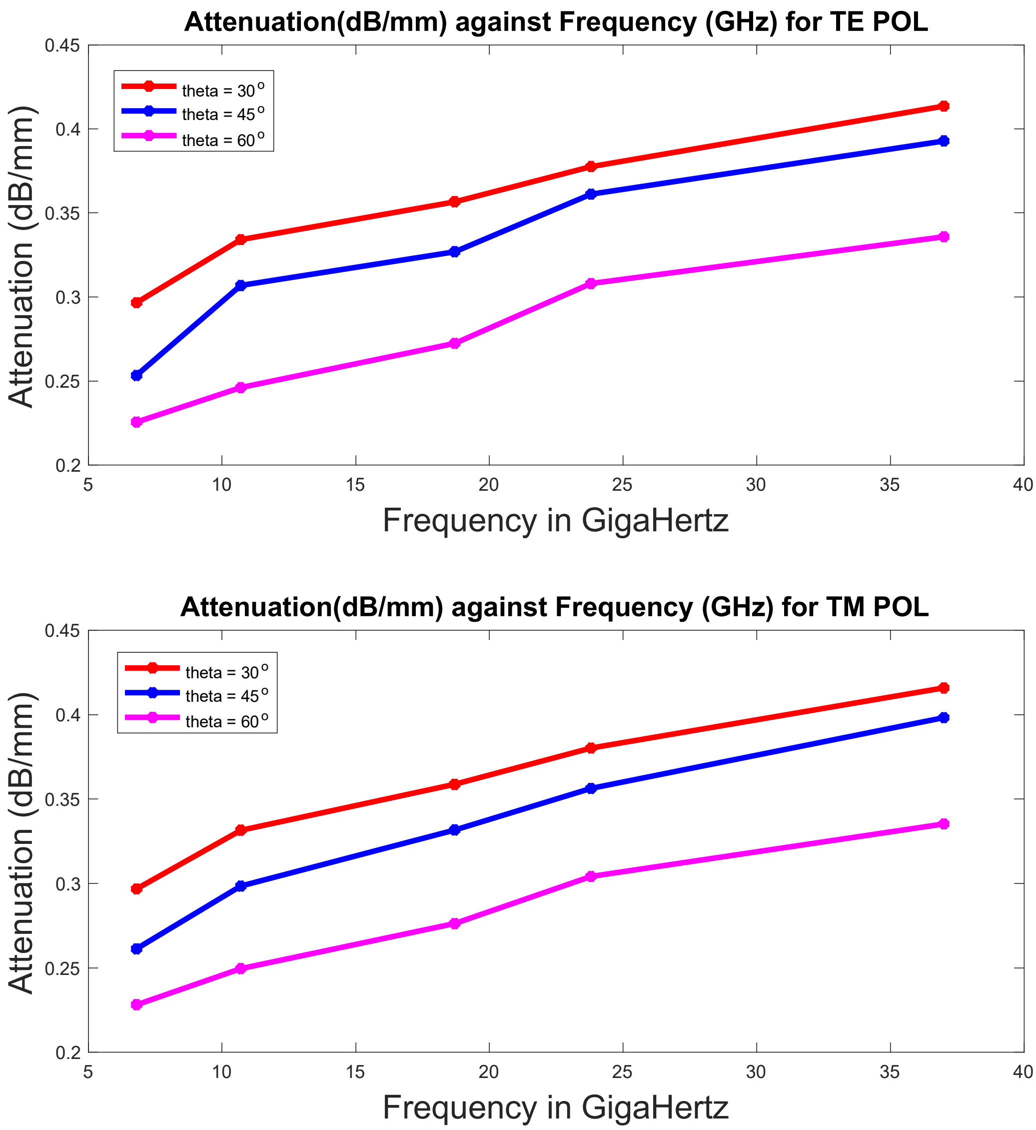

Figure 4. Specific attenuation (dB/mm) against frequency (GHz) with propagation angles zenith θ_i= 30°, 45° and 60° for thin phase scattering screens

Attenuation α_{dB} of the field intensity $|E|^2$ for both TE and TM polarize fields increases with increase in frequency and depth of sea foam layer for thin phase screens $\delta_t = 0.1\, mm$ and $\delta_t = 0.2\, mm$, with zenith $\theta_i = 30^{\circ}$ and azimuth $\emptyset = 0^{\circ}$ as shown in figure 1. The attenuation α_{dB} is highest at $37\, GHz$ with a value of $\alpha_{dB} = 6.1695\, dB$ for TE mode and $\alpha_{dB} = 6.1199\, dB$ for TM mode. We have an attenuation of $0\, dB$ at slice 1, $1.5384\, dB$ at slice 2, $3.2864\, dB$ at slice 3, $4.6431 dB$ at slice 4 and $5.0390\, dB$ at slice 5 and $6.1695\, dB$ at the sea-surface for TE polarize field. Similarly, attenuation at slice 1 is $0\, dB$, $1.5649\, dB$ at slice 2, $3.3080\, dB$ at slice 3, $4.7179\, dB$ at slice 4 and $5.0797\, dB$ at slice 5 and $6.11695\, dB$ at the sea-surface for TM polarize field. The attenuation α_{dB} at $6.8\, GHz$ gives the least variation of attenuation with depth as shown in figure 2. We obtain an attenuation $\alpha_{dB} = 0\, dB$ at slice 1, $\alpha_{dB} = 1\, dB$ at slice 2, $\alpha_{dB} = 2.2969\, dB$ at slice 3, $\alpha_{dB} = 3.0210\, dB$ at slice 4, $\alpha_{dB} = 4.0385\, dB$ at slice 5 and $\alpha_{dB} = 4.4751\, dB$ at the sea surface for TE polarize field and $\alpha_{dB} = 0\, dB$ at slice 1, $\alpha_{dB} = 1\, dB$ at slice 2, $\alpha_{dB} = 2.2820\, dB$ at slice 3, $\alpha_{dB} = 3.0065\, dB$ at slice 4, $\alpha_{dB} = 4.0539\, dB$ at slice 5 and $\alpha_{dB} = 4.4970\, dB$. It is apparent that the attenuation at various WindSat frequencies (6.8GHz − 37GHz) increases with depth of sea foam layer for thin phase scattering screens. The plots in figure 4 shows that attenuation also reduces with increase in zenith angle θ_i from 30° to 60° for both TE and TM polarize fields. We observe that as θ_i approaches 90°, the attenuation reduces due to weaker interaction between the E-field and randomly distributed scatterers. There is more diffuse scattering at smaller angle of incidence and multiple reflections in sea foam layer increases with frequency at deeper sea foam layers. For thin-phase scattering screens $\delta_t = 0.1\, mm$ and $\delta_t = 0.2\, mm$ with a given zenith $\theta_i = 60^{\circ}$ and azimuth $\emptyset = 0^{\circ}$, the attenuation α_{dB} increases with depth $d\ (mm)$ of sea foam. Figure 4 shows this to be true for all WindSat frequencies ($6.8 - 37$GHz) as the E-field travels through successive slices of sea foams. For both TE and TM polarized fields, the attenuation α_{dB} at $\theta_i = 60^{\circ}$ is less than that of $\theta_i = 30^{\circ}$ and $\theta_i = 30^{\circ}$. This agrees with earlier report that the attenuation due to backscattered E-field by foam covered sea-surface reduces with increase in angle of incidence.

CONCLUSION

We were able to illustrate that extinction of propagated E-field through thin phase scattering screens are due to diffused reflections by the sea foam covered sea-surface which builds up as the E-field travels further through the slices of the sea foam layers. For deep phase scattering screens, the E-field is absorbed within the sea foam layer as it travels further through the deep phase screens. These behaviours of the E-field extinction are dependent on the frequency of the propagated field, the slice thickness □□, the depth of sea foam layer, effective dielectric constant of sea foam, foam void fraction and incident angle of propagating E-field.

REFERENCES

Anguelova, M. D. 2008. "Complex Dielectric Constant of Sea Foam at Microwave Frequencies", Journal of Geophysical Research, Vol. 133, C08001, 2008.

Anguelova, M. D. M. Bettenhausen, and P. Gaiser. "Passive remote sensing of sea foam using physically-based models", *2006 IEEE International Symposium on Geoscience and Remote Sensing*, IEEE, 2006.

Anguelova, M. D. "Passive remote sensing of oceanic whitecaps: Further developments", *AGU Fall Meeting Abstracts*. 2013.

Stogryn, A. "The emissivity of sea foam at microwave frequencies", *Journal of Geophysical Research,* vol. 77, no. 9, 1658–1666, 1972.

Xiaobin, Y. et al. "Optimization of L-band sea surface emissivity models deduced from SMOS data." *IEEE Transactions on Geoscience and Remote Sensing*, vol. 50.5, pp. 1414-1426, 2012.

Chen, D. L. Tsang, L. Zhou, S. C. Reising, W. E. Asher, L. A. Rose, K.-H. Ding, and C.- T. Chen, "*Microwave emission and scattering of foam based on Monte-Carlo simulations of dense media",* Geoscience and Remote sensing, *IEEE Transanction on*, vol. 41, no. 4, 782–790, 2003.

****